

All-optical control of the quantum flow of a polariton condensate

D. Sanvitto^{1*}, S. Pigeon², A. Amo^{3,4}, D. Ballarini⁵, M. De Giorgi¹, I. Carusotto⁶, R. Hivet³, F. Pisanello³, V. G. Sala³, P. S. S. Guimaraes⁷, R. Houdré⁸, E. Giacobino³, C. Ciuti², A. Bramati³ and G. Gigli^{1,5,9}

Although photons in vacuum are massless particles that do not appreciably interact with each other, significant interactions appear in suitable nonlinear media, leading to hydrodynamic behaviours typical of quantum fluids^{1–6}. Here, we show the generation and manipulation of vortex-antivortex pairs in a coherent gas of strongly dressed photons (polaritons) flowing against an artificial potential barrier created and controlled by a light beam in a semiconductor microcavity. The optical control of the polariton flow allows us to reveal new quantum hydrodynamical phenomenologies such as the formation of vortex pairs upstream from the optical barrier, a case of ultra-short time excitation of the quantum flow, and the generation of vortices with counterflow trajectories. Additionally, we demonstrate how to permanently trap and store quantum vortices hydrodynamically generated in the wake of a defect. These observations are supported by time-dependent simulations based on the non-equilibrium Gross-Pitaevskii equation⁷.

Bosonic quasi-particles that emerge in a semiconductor microcavity from the strong coupling of confined photons and quantum well excitons are commonly called polaritons⁸. The exciton component provides efficient polariton-polariton interactions, which result in strong optical nonlinearities, and the photonic component allows for the direct generation, manipulation and observation of polariton gases with optical techniques. Compared to standard quantum fluids such as liquid helium or ultracold atomic gases, polariton fluids are expected to show new interesting non-equilibrium effects originating from the finite lifetime of the constituent particles and the driven-dissipative nature of the optical fluid^{9,10}.

As bosonic particles, polaritons have recently been demonstrated to undergo a phase transition to a Bose-condensed state^{11,12}. This has triggered the search for superfluid behaviours in polariton gases, opening up new exciting possibilities. Recently, the study of nonlinear flow phenomena in polaritons has led to the observation of superfluidity^{13–15}, persistent circular flows¹⁶ and hydrodynamic nucleation of dark solitons^{7,17}. Photon-based polariton fluids, in particular, appear to be the most promising candidates for the study of quantum hydrodynamic effects and topological excitations such as vortices of quantized angular momentum. These quanta of circulation lie in a multi-dimensional Hilbert space, so there is interest in the possibility of using them, for instance, as qudits¹⁸—qubits in a higher dimensional system—as proposed for the case of purely photonic vortices^{19,20}. In this context, polariton condensates may have the advantage of having large intrinsic nonlinearities as well as already being integrated in semiconductor chips.

A quantum fluid encountering different kinds of obstacles may break its superfluid regime by the emission of topological excitations (vortices). This effect has recently been studied in ultracold atoms^{21,22}, and in a gas of resonantly generated polaritons hitting a natural defect in a sample⁶. In this Letter, we take advantage of strong polariton nonlinearities to optically create obstacle potentials of tunable shape and height. In particular, we demonstrate the possibility of fully controlling vortex nucleation and motion by optical means, as well as of permanently storing pairs of vortices in a suitably tailored optical trap. This is a crucial advance over the first experiments showing optical vortices in planar microcavity lasers²³ and in polariton condensates, where pinned vortices spontaneously appear in the disordered potential of the cavity²⁴ or in the minima of the excitation laser field²⁵.

Figure 1 shows the typical lower polariton dispersion of a microcavity under strong photon-exciton coupling (see Methods). The polariton condensate is excited by a resonant laser with linear polarization and a finite in-plane wave vector (red arrow in Fig. 1a). The in-plane wave vector results in a finite flow velocity of the polariton fluid. To avoid any effect of the laser field and phase on flow propagation, we mask half of the laser spot. In this configuration, the phase of the superfluid is not locked to that of the laser, and is therefore free to evolve in space and time. Note that if this mask is absent, as in ref. 6, any inhomogeneity of the pumping laser, close to the obstacle, could strongly influence the fluid dynamics and the appearance of topological defects²⁵.

The artificial potential barrier is created by a continuous-wave (c.w.) laser (Fig. 1b), with linear polarization orthogonal to that of the pumping pulsed laser (see Methods). Details of the sample used and the time-resolved techniques for detecting the polariton flow and its barrier-induced excitations are described in the Supplementary Information.

Figure 2 shows five temporal snapshots of the real space density and phase profile of a polariton condensate injected in the cavity with a rightward supersonic speed ($c_s < v_f$) of $v_f = 1.1 \mu\text{m ps}^{-1}$. The shape of the barrier is Gaussian (diameter, $\sim 10 \mu\text{m}$; mean height, 0.4 meV), and its position is indicated by a blue circle. The successive snapshots show the formation of a pair of vortices with opposite circulation in the centre of the fluid 10 ps after the arrival of the pulse and upstream from the position of the defect. In the subsequent 10 ps, the vortex and antivortex are pushed away from the centre of the potential barrier towards its sides at a velocity of $\sim 0.9 \mu\text{m ps}^{-1}$. However, after the vortices have reached the equator of the obstacle, there is a clear deceleration of

¹NNL, Istituto Nanoscienze - CNR, Via Arnesano, 73100 Lecce, Italy, ²Laboratoire Matériaux et Phénomènes Quantiques, UMR 7162, Université Paris Diderot-Paris 7 et CNRS, 75013 Paris, France, ³Laboratoire Kastler Brossel, Université Pierre et Marie Curie-Paris 6, École Normale Supérieure et CNRS, UPMC Case 74, 4 place Jussieu, 75005 Paris, France, ⁴CNRS-Laboratoire de Photonique et Nanostructures, Route de Nozay, 91460 Marcoussis, France, ⁵Istituto Italiano di Tecnologia, IIT-Lecce, Via Barsanti, 73010 Lecce, Italy, ⁶INO-CNR BEC Center and Dipartimento di Fisica, Università di Trento, I-38123 Povo, Italy, ⁷Departamento de Física, Universidade Federal de Minas Gerais, Belo Horizonte MG, Brazil, ⁸Institut de Physique de la Matière Condensée, Faculté des Sciences de Base, bâtiment de Physique, Station 3, EPFL, CH-1015 Lausanne, Switzerland, ⁹Dipartimento Ing. Innovazione, Università del Salento, Via Arnesano, 73100 Lecce, Italy. *e-mail: danielle.sanvitto@nano.cnr.it

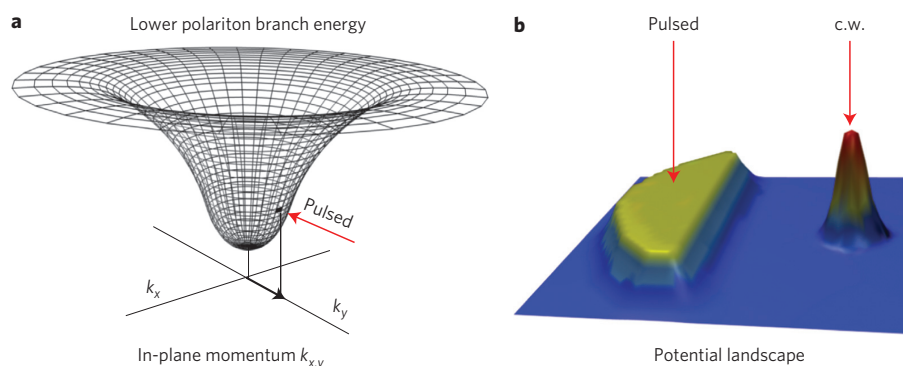


Figure 1 | Schematic of the experiment. **a**, Lower polariton dispersion with a red arrow indicating the pulsed laser wave vector. **b**, Sketch of the bare polariton potential landscape, strongly modified by both the pulsed laser injecting the polariton flow (almost flat due to saturation effects) and by the c.w. laser giving rise to the artificial potential barrier.

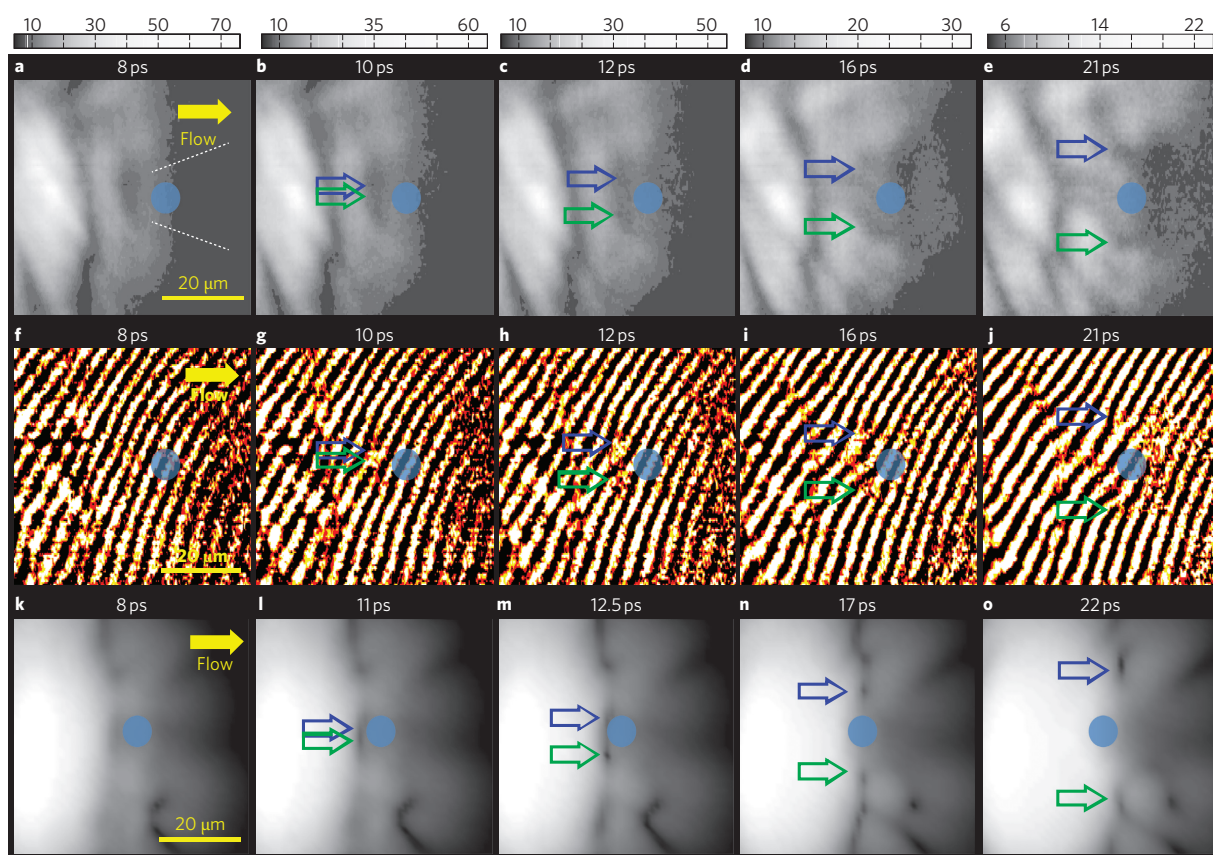


Figure 2 | Effect of the optical barrier on the nucleation of vortex-antivortex pairs. **a-e**, Snapshots of the real space emission pattern of the polariton fluid (power of the pulsed laser, $P_{\text{pulsed}} = 4 \text{ mW}$) hitting an optical defect (blue circle, c.w. laser power $P_{\text{c.w.}} = 26 \text{ mW}$) at different times after the pulse. The dark vertical contour originates from the redshifted region created by the sharp edge of the masked laser spot. The dotted lines show the angle of the shock waves. **f-j**, Corresponding interferograms giving the spatial profile of the condensate phase. Vortices are revealed as density minima corresponding to their core in **b-e**, and as fork-like dislocations in the interferograms shown in **g-j**. **k-o**, Theoretical simulations using the parameters of the experimental images (**a-e**). The blue and green arrows indicate the positions of the vortex-antivortex as these are dragged by the fluid. Real-space images are in logarithmic colour scales.

their motion and a small excursion along the vertical axis orthogonal to the flow direction.

Remarkably, unlike the observations in refs 6, 21, 22, 26 and 27, the formation of vortices takes place at a position just upstream of the defect and not in its wake. Those other works considered a flow hitting a deep and spatially abrupt potential, but in the present experiments we optically generate a potential with a smooth profile and a relatively shallow depth, which therefore

allows the condensate to partially penetrate the obstacle. As a result, the nucleation of the vortex pair happens upstream of the barrier, apparently at the position where the local fluid velocity approaches the sound velocity, which is the usual condition for vortex nucleation. Note that this condition is satisfied in our experiment upstream of the defect, and not downstream as in previous experiments^{6,22}. This remarkable fact is confirmed by the solution of the time-dependent non-equilibrium Gross-Pitaevskii

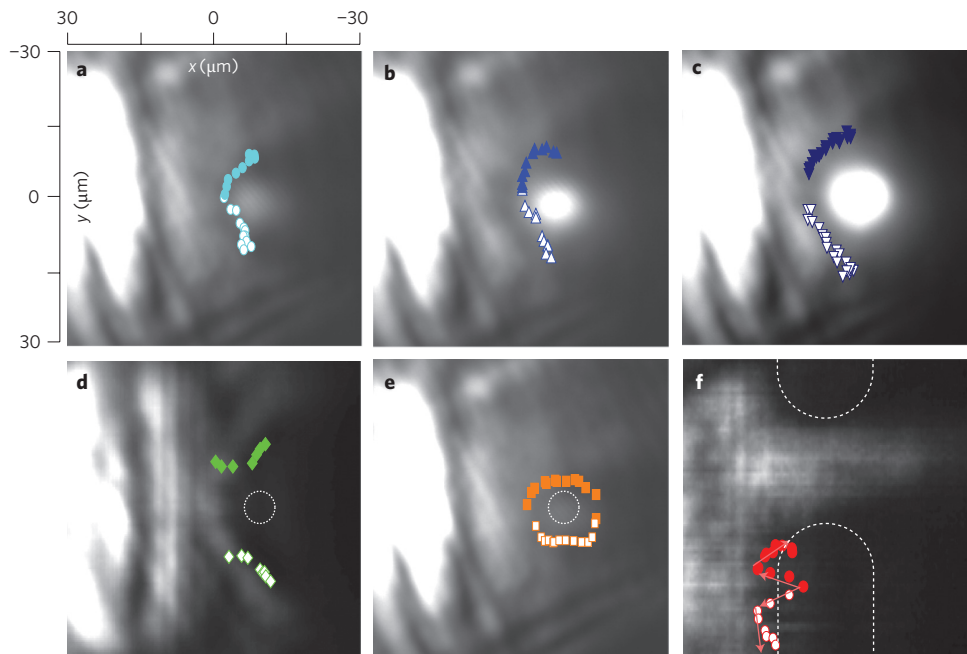


Figure 3 | Time-integrated real space emission patterns and corresponding vortex trajectories (obtained from successive time shots) for different parameters of the c.w. laser, injection density and barrier shape. Vortex trajectories are from left to right. **a–c,e**, Results with a fixed pulse power, $P_{\text{pulsed}} = 4$ mW, and different c.w. powers, $P_{\text{cw}} = 6$ mW (**a**), 26 mW (**b**), 52 mW (**c**) and 2 mW (**e**). **d**, Results with the same potential barrier as in **b**, but with higher pump intensity $P_{\text{pulsed}} = 14$ mW. **f**, The optical defect is shaped into an infinitely long barrier with a ~ 20 μm channel (boundaries shown by dotted lines). Here, the vortex trajectory shows an opposite behaviour from right to left (pushed back by the barrier), then following the flow as indicated by the arrows.

equations with the actual experimental excitation conditions (Fig. 2, third row, and Supplementary Information).

A more detailed analysis of the vortex trajectories for different conditions of the optical barrier and densities of injected polaritons is shown in Fig. 3. Increasing the c.w. power (Fig. 3a–c) results in an increase in both the height and effective width of the potential experienced by the moving polaritons. A larger diameter of the potential would tend to push the vortex–antivortex nucleation point upstream, closer to the pulse injection area, where the density is higher, giving a higher sound speed c_s . When this happens, nucleation tends to occur further away from the obstacle axis, at positions where the local flow velocity tangential to the obstacle is higher, and the condition $v_f = c_s$ is satisfied. This is confirmed by the theoretical analysis shown in Supplementary Fig. 2S. To further assess the effect of the change in polariton density on the interaction with the defect, we repeated the experiment with a higher power for the pulsed laser (Fig. 3d) so as to inject a higher density of polaritons— $39.8 \mu\text{m}^{-2}$ ($c_s = 0.8 \mu\text{m ps}^{-1}$), in contrast to $12.4 \mu\text{m}^{-2}$ ($c_s = 0.4 \mu\text{m ps}^{-1}$) of Fig. 3b—but keeping similar values for the barrier height and size. Under this condition, the nucleation point shifts towards the edge of the barrier, where the flow velocity is higher^{26,27}. Even though the increase in the density is slightly compensated by a higher fluid velocity of the injected polaritons ($v_f = 1.4 \mu\text{m ps}^{-1}$), the dominant effect is in the variation of the speed of sound, giving an increase of 25% in c_s/v_f relative to the experiment in Fig. 3c.

Another interesting outcome is observed with a very small defect size (Fig. 3e). Here, the vortex–antivortex pair follows the contour of the obstacle and then recombines downstream from the defect. In this case, owing to the reduced dimension of the defect, the polariton density is not strongly reduced in the wake of the potential, allowing for the observation of vortex/antivortex annihilation once the flow has recovered its unperturbed pathway. This remarkable result shows the ultrashort lifetime of a topological excitation created on the quantum fluid, which continues to keep an unperturbed stream before and after the

defect in the form of laminar flow of a quantum fluid (see Supplementary video).

Figure 3f presents the results when we changed the shape of the obstacle into a rectangular extended barrier with a ~ 20 μm channel through which polaritons were able to flow. Interestingly we observe the formation of a vortex pair at the boundary of the optical barrier, which is first scattered back, reflected by the barrier itself, and subsequently pushed forward by the polariton condensate flowing towards the channel for the vortex, and along the barrier for the antivortex. This shows the extraordinary variety of phenomenology and dynamics of vortex pairs obtained by means of simple manipulation of the optical defect.

So far, we have shown that an artificial, optically induced, potential barrier is able to produce the hydrodynamic nucleation of vortices in a flowing polariton fluid. However, these vortices can only last for as long as the polariton fluid survives in the cavity. An alternative strategy to make vortices last for times much longer than the polariton lifetime is to work under a c.w. excitation and to use a suitably tailored mask to nucleate and then trap vortex pairs, as theoretically suggested in ref. 7.

This proposal is experimentally demonstrated in Fig. 4. Polaritons with a well-defined momentum were injected by a single c.w. laser and directed against a potential barrier (here formed by a natural defect present in the microcavity). In the absence of a mask (Fig. 4a), the phase of the polariton fluid is locked to that of the pump laser, so that vortices are prevented from nucleating, even at supersonic speeds. On the other hand, when a dark region is placed right downstream of the defect (dark triangle in Fig. 4b), pairs of vortices that are hydrodynamically nucleated in the proximity of the defect can freely penetrate in the dark area where the polariton phase is not locked by the incident laser (note the phase dislocations in Fig. 4h). As the phase of the fluid is homogeneous outside the triangle, phase matching prevents vortices from diffusing out and they become permanently trapped within the triangular borders. Moving the dark region slightly away from the defect, we can still

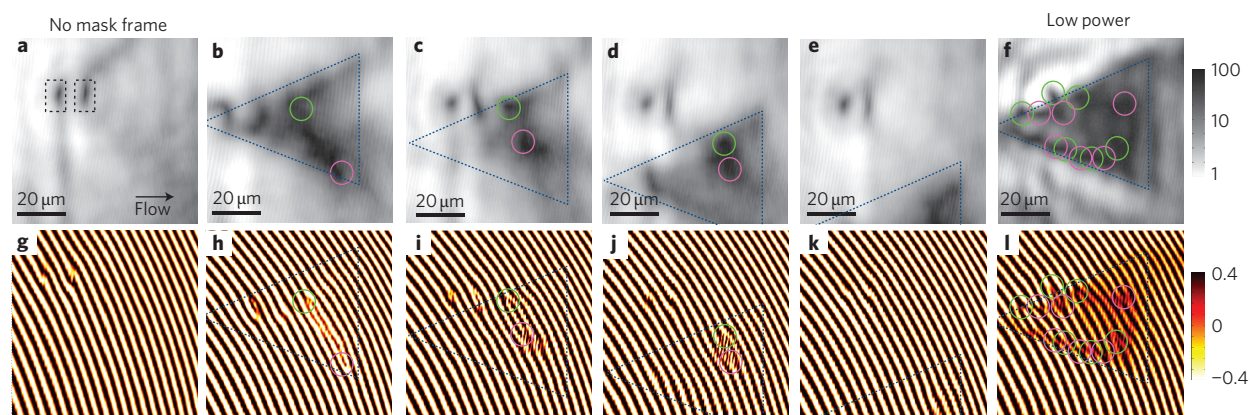


Figure 4 | Vortex-antivortex pair storage in a triangular trap. **a–f**, Real-space images (**a–f**) and corresponding interferograms (**g–l**) for polaritons injected by a c.w. laser beam and flowing against a natural defect in the microcavity (marked by rectangles in **a**). In **ag**, the spot is larger than the field of view and no mask is applied: the density is uniform behind the defect and phase is pinned. In **b**, a triangular dark region within the excitation spot is created behind the defect and two pairs of vortices (green and magenta) become trapped inside this region: see the forks in **h**. In **c–e** and **i–k**, the mask is laterally shifted with respect to the optical defect. In **e,k**, the mask is shifted far away from the defect and vortex nucleation is frustrated due to the homogeneous phase imprinted by the pump laser. In **fl** the pumping power of the laser is lowered to allow for many vortex pairs to become trapped.

observe the presence of some trapped vortices within this area (Fig. 4c,d,i,j). On the other hand, if the dark trap is moved away from the cone set by the shock waves (appreciable in Fig. 4a), vortices cannot get trapped inside the triangle and their appearance remains frustrated by the homogeneous phase imprinted by the pump laser (Fig. 4e,k).

The capacity of storage (number of vortices per unit area) is strongly determined by the strength of the laser field leaking inside the triangular region⁷. Indeed, for sufficiently high intensities of the resonant c.w. laser, the amount of light diffracted by the edges of the metallic mask is sufficient to partially fix the laser phase in a part of the inner region, as is the case in Fig. 4b,c,d where only a pair of vortices is present. However, by reducing the total laser power, the speed of sound in the fluid and the light field inside the triangle drop, and the number of vortices trapped by the masked region proliferate, as shown in Fig. 4f, mainly along the edges of the triangle. This observation demonstrates the possibility of storing a controlled number of vortices. Note that, in principle, the vortex pairs could be retained inside the triangle for as long as the c.w. laser is on.

Our experiments show the potential of optical methods for the study, generation and manipulation of quantized vortices in a quantum fluid. We show that we can fully control the obstacle parameters by means of laser-induced artificial potentials, allowing us to inspect the physics of the vortex nucleation process in unconventional regimes and revealing new effects such as the formation upstream of the defect and the ultrashort reversible excitation of a quantum fluid. We further demonstrate the possibility of trapping and storing vortices in an all-optical way by using a triangular, optically induced potential. Our observations confirm that polariton condensates are an alternative to ultracold atoms²⁸ for the study of hydrodynamic turbulence effects²⁹ in new regimes, and using solid-state samples that are operational up to room temperature³⁰. The all-optical control and trapping of vortices sets the basis for the study of optical vortex lattices and their excitations.

Methods

In the present experiment, polaritons were coherently created in a planar semiconductor microcavity by resonantly exciting the sample with a pulsed Ti:sapphire laser. The sample is described in detail in ref. 15 and in the Supplementary Information. To avoid the detrimental effect of the excitation laser phase we used the scheme proposed in ref. 7, in which half of the laser spot was masked to allow penetration of the propagating polariton flow in a region clear from the pumping laser.

Time-resolved real-space images of the polariton field were obtained in transmission geometry with the use of a synchroscan streak camera. The real-space phase pattern of the polariton field was inferred from interferograms resulting from the interference of the cavity emission with a reference beam of constant phase coming from the pulsed laser itself.

The barriers were generated by a c.w. laser with cross-polarized field and a pulsed laser that generated the polariton flow. This c.w. beam was normally incident to the sample and its frequency was resonant with the bottom of the polariton dispersion at $k_{\parallel} = 0$. Its purpose was to introduce in the spot region a steady population of exciton-polaritons large enough to locally result in a significant blueshift of the polariton states under the effect of interparticle interactions. This was demonstrated to give rise to two populations that behaved independently in the case of resonant c.w. excitation³¹; however, it has never been implemented and proved to act as a potential obstacle in a non-steady-state system where polaritons are truly flowing, independently from the exciting laser beams. By varying the c.w. intensity, blueshifts ranging from 0.1 to 0.8 meV were obtained. The size and shape of the potential obstacle were controlled simply by the size and shape of the c.w. laser spot (Fig. 1 shows a scheme of such a potential landscape). In the images shown in Figs 2 and 3, we isolated the emission coming from the flowing polaritons injected by the pulsed laser using suitable polarizers and with time-resolved experiments. In this way, the contribution of the cross-polarized c.w. laser (needed to create the obstacle) was minimized.

In Fig. 2, the images are time snapshots obtained by integrating over several millions of experiments. The background images of Figs 3 and 4 are time-integrated (~ 1 s) for the entire duration of the experiment.

Received 16 March 2011; accepted 23 July 2011;
published online 11 September 2011

References

- Carusotto, I. & Ciuti, C. Swimming in a sea of superfluid light. *Europhys. News* **41**, 23–27 (2010).
- Couillet, P., Gil, L. & Rocca, F. Optical vortices. *Opt. Commun.* **73**, 403–408 (1989).
- Staliunas, K. & Sanchez-Morcillo, V. J. *Transverse Patterns in Nonlinear Optical Resonators* (Springer-Verlag, 2003).
- Wan, W., Jia, S. & Fleischer, J. W. Dispersive superfluid-like shock waves in nonlinear optics. *Nature Phys.* **3**, 46–51 (2007).
- Bolda, E. L., Chiao, R. Y. & Zurek, W. H. Dissipative optical flow in a nonlinear Fabry-Perot cavity. *Phys. Rev. Lett.* **86**, 416–419 (2001).
- Nardin, G. et al. Hydrodynamic nucleation of quantized vortex pairs in a polariton quantum fluid. *Nature Phys.* **7**, 635–641 (2011).
- Pigeon, S., Carusotto, I. & Ciuti, C. Hydrodynamic nucleation of vortices and solitons in a resonantly excited polariton superfluid. *Phys. Rev. B* **83**, 144513 (2011).
- Kavokin, A., Baumberg, J. J., Malpuech, G. & Laussy, F. P. *Microcavities* (Oxford Univ. Press, 2007).
- Szymanska, M. H., Keeling, J. & Littlewood, P. B. Nonequilibrium quantum condensation in an incoherently pumped dissipative system. *Phys. Rev. Lett.* **96**, 230602 (2006).
- Wouters, M. & Carusotto, I. Superfluidity and critical velocities in nonequilibrium Bose-Einstein condensates. *Phys. Rev. Lett.* **105**, 020602 (2010).

11. Kasprzak, J. *et al.* Bose–Einstein condensation of exciton polaritons. *Nature* **443**, 409–414 (2006).
12. Balili, R., Hartwell, V., Snoke, D., Pfeiffer, L. & West, K. Bose–Einstein condensation of microcavity polaritons in a trap. *Science* **316**, 1007–1010 (2007).
13. Amo, A. *et al.* Collective fluid dynamics of a polariton condensate in a semiconductor microcavity. *Nature* **457**, 291–295 (2009).
14. Carusotto, I. & Ciuti, C. Probing microcavity polariton superfluidity through resonant Rayleigh scattering. *Phys. Rev. Lett.* **93**, 166401 (2004).
15. Amo, A. *et al.* Superfluidity of polaritons in semiconductor microcavities. *Nature Phys.* **5**, 805–810 (2009).
16. Sanvitto, D. *et al.* Persistent currents and quantized vortices in a polariton superfluid. *Nature Phys.* **6**, 527–533 (2010).
17. Amo, A. *et al.* Polariton superfluids reveal quantum hydrodynamic solitons. *Science* **332**, 1167–1170 (2011).
18. Cerf, N. J., Bourennane, M., Karlsson, A. & Gisin, N. Security of quantum key distribution using *d*-level systems. *Phys. Rev. Lett.* **88**, 127902 (2002).
19. Molina-Terriza, G., Torres, J. P. & Torner, L. Twisted photons. *Nature Phys.* **3**, 305–310 (2007).
20. Mair, A., Vaziri, A., Weihs, G. & Zeilinger, A. Entanglement of the orbital angular momentum states of photons. *Nature* **412**, 313–316 (2001).
21. Inouye, S. *et al.* Observation of vortex phase singularities in Bose–Einstein condensates. *Phys. Rev. Lett.* **87**, 080402 (2001).
22. Neely, T. W., Samson, E. C., Bradley, A. S., Davis, M. J. & Anderson, B. P. Observation of vortex dipoles in an oblate Bose–Einstein condensate. *Phys. Rev. Lett.* **104**, 160401 (2010).
23. Scheuer, J. & Orenstein, M. Optical vortices crystals: spontaneous generation in nonlinear semiconductor microcavities. *Science* **285**, 230–233 (1999).
24. Lagoudakis, K. G. *et al.* Quantized vortices in an exciton–polariton condensate. *Nature Phys.* **4**, 706–710 (2008).
25. Roumpos, G. *et al.* Single vortex–antivortex pair in an exciton–polariton condensate. *Nature Phys.* **7**, 129–133 (2011).
26. Frisch, T., Pomeau, Y. & Rica, S. Transition to dissipation in a model of superflow. *Phys. Rev. Lett.* **69**, 1644–1647 (1992).
27. Winiecki, T., Jackson, B., McCann, J. F. & Adams, C. S. Vortex shedding and drag in dilute Bose–Einstein condensates. *J. Phys. B* **33**, 4069–4078 (2000).
28. Henn, E. A. L. *et al.* Emergence of turbulence in an oscillating Bose–Einstein condensate. *Phys. Rev. Lett.* **103**, 045301 (2009).
29. Berloff, N. G. Turbulence in exciton–polariton condensates. Preprint at <http://arxiv.org/abs/1010.5225> (2010).
30. Christopoulos, S. *et al.* Room-temperature polariton lasing in semiconductor microcavities. *Phys. Rev. Lett.* **98**, 126405 (2007).
31. Amo, A. *et al.* Light engineering of the polariton landscape in semiconductor microcavities. *Phys. Rev. B* **82**, 081301 (2010).

Acknowledgements

This work was partially supported by the Agence Nationale pour la Recherche (GEMINI 07NANO 07043), the IFRAF (Institut Francilien pour les atomes froids), project MIUR FIRB ItalNanoNet and the POLATOM ESF Research Networking Program. I.C. acknowledges financial support from the ERC through the QGBE grant. P.S.S.G. acknowledges support from CNPq, Brazil. A.B. and C.C. are members of the Institut Universitaire de France (IUF). The authors are grateful to G. Martiradonna for helping with the realization of the laser mask and to P. Cazzato for technical support.

Author contributions

All authors contributed to the implementation and modelling of the experiment, interpretation of the results and writing of the manuscript.

Additional information

The authors declare no competing financial interests. Supplementary information accompanies this paper at www.nature.com/naturephotonics. Reprints and permission information is available online at <http://www.nature.com/reprints>. Correspondence and requests for materials should be addressed to D.S.